Table 1. Variant priority scheme after exome sequencing[a]

	NEXTGENE	II-2	MAQ (SEATTLESEQ)
Total variants called	22,176	—	58,081
Chr X	3441	—	4383
Unknown SNP variants	910	—	882
(dbSNP131, 1000 genomes)	—	—	—
Overlap of NEXTGENE and MAQ	—	169	—
NS/SS	—	17	—
Except for variants at segmental duplications	—	15	—

NS, non-synonymous; SNP, single-nucleotide polymorphism; SS, splice site (±2).
[a]MAQ was annotated with SEATTLESEQ ANNOTATION. The annotation includes gene names, dbSNP rs ID, and SNP functions (e.g. missense), protein positions and amino acid changes.

cell for II-2 (Illumina). Image analyses and base calling were performed using sequence control software real-time analysis and OFFLINE BASECALLER software v1.8.0 (Illumina). Reads were aligned to the human reference genome (UCSC hg19, NCBI build 37.1).

Mapping strategy and variant annotation

The quality-controlled (Path Filter) reads were mapped to the human reference genome (UCSC hg19, NCBI build 37.1), using mapping and assembly with quality (MAQ) and NEXTGENE software v2.0 (SoftGenetics, State College, PA). Single-nucleotide polymorphisms in MAQ-passed reads were annotated using the SEATTLESEQ ANNOTATION website (http://gvs.gs.washington.edu/SeattleSeqAnnotation/).

Priority scheme and capillary sequencing

Called variants found by each informatics method were filtered in terms of location on chromosome X, unregistered variants (excluding registered dbSNP131 and 1000 Genomes), overlapping variants called in common by NEXTGENE and MAQ, and non-synonymous changes and splice-site mutations (±2 bp from exon–intron junctions) (Table 1). The variants were confirmed as true positives by Sanger sequencing of polymerase chain reaction (PCR) products amplified using genomic DNA as a template, except for variants within genes at segmental duplications. Sanger sequencing was performed on an ABI3500xl or ABI3100 autosequencer (Life Technologies, Carlsbad, CA). Sequencing data were analyzed using SEQUENCHER software (Gene Codes Corporation, Ann Arbor, MI).

Reverse transcription-PCR

Total RNA was isolated from EBV-transformed lymphoblastoid cell line (EBV-LCL) derived from II-2 and healthy control subjects using the RNeasy Plus Mini Kit (QIAGEN). Five micrograms of total cellular RNA was used for reverse transcription with the Super Script III First-Strand Synthesis System (Life Technologies). Two microliters of synthesized complementary DNA was used for PCR with the following primers: ex17-F (5′-CTACCATCACCCACTGAGTC-3′) and ex19-R (5′-TGAGACATATCCCCGGCAG-3′). Amplified PCR products were electrophoresed in agarose gels, purified from gels using the QIAquick Gel Extraction Kit (QIAGEN), cloned into pCR4-TOPO vector (Life Technologies) and sequenced.

X-chromosome inactivation assay

The human androgen receptor (HUMARA) assay was performed as previously reported (9). Genomic DNA of II-2 was digested at 37°C for 18 h with two methylation-sensitive enzymes, *Hpa*II and *Hha*I. PCR was performed using digested and undigested DNA with HUMARA primers (FAM-labeled ARf: 5′-TCCAGAATCTGTTCCAGAGCGTGC-3′; ARr: 5′-CTCTACGATGGGCTTGGGGAGAAC-3′). DNA fragment analysis was performed on an ABI3130xl autosequencer (Life Technologies). Fragment data were analyzed with GENEMAPPERT SOFTWARE version 4.1 (Life Technologies).

Results

Exome sequencing

Because this disorder was assumed to be an 'X-linked recessive' disorder based on the initial pedigree information, we focused on the X chromosome. Approximately 4.5 Gb of sequence data were generated, 87.3% of which was mapped to the human reference genome (UCSC hg19, NCBI build 37.1). MAQ was able to align 53,242,972 reads to the whole genome.

Two informatics methods identified 17 potential pathogenic changes (15 missense mutations, 1 nonsense mutation, and 1 splice-site mutation) (Table 1). The nonsense mutation was a false positive and all 13 missense mutations were inconsistent with the phenotype (no co-segregation). The mutation c.2388+1G>C was identified at the splice-acceptor site of intron 17 in *OFD1*, heterozygously in II-2, and hemizygously in III-5, but was absent in II-3, III-3, and III-6 (Fig. 3a) as well as 93 normal female controls (0/186 alleles).

RT-PCR, direct sequencing

To examine the mutational effects of c.2388+1G>C, reverse transcriptase-polymerase chain reaction (RT-PCR) was performed. Only a 239-bp PCR product (wild-type allele) was observed in healthy control individuals (Fig. 3b). By contrast, a longer 1364-bp product was detected in II-2. Sequencing of the 1364-bp product revealed that a 1125-bp sequence of intron 17 was retained, producing a premature stop codon at amino acid position 796 (Fig. 3b). These data indicate

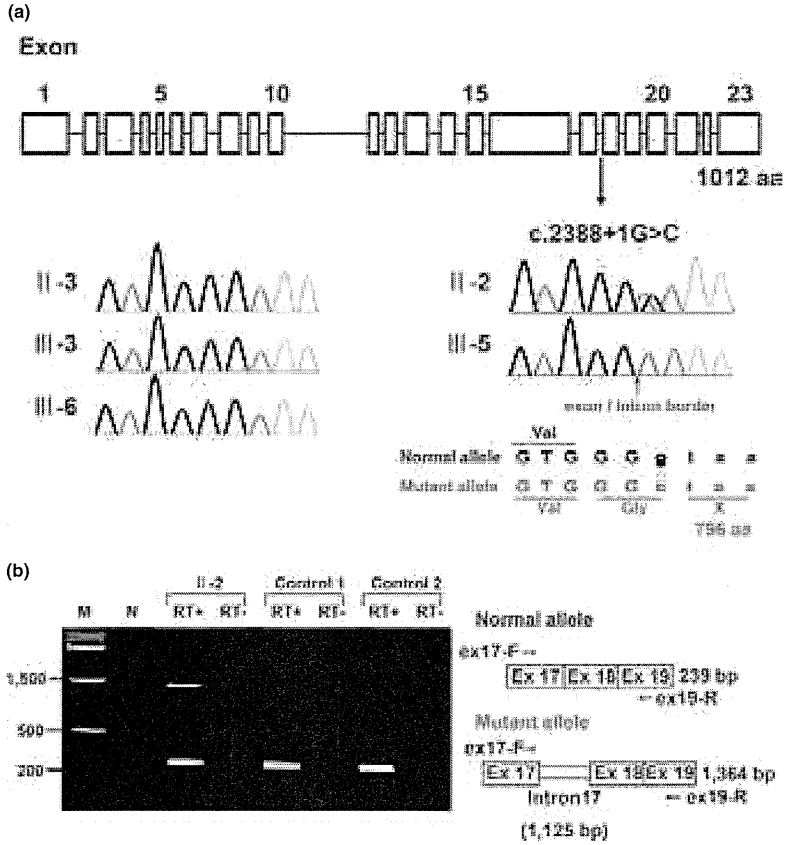

Fig. 3. (**a**) Gene structure of *OFD1* with the mutation (c.2388+1G>C) (upper). Electropherograms of the family members. Wild-type sequences are seen in II-3, III-3 and III-6. Heterozygous and hemizygous mutations are observed in II-2 and III-5, respectively. (**b**) Reverse transcriptase-polymerase chain reaction analysis showing both 239-bp and 1364-bp products in II-2, and only 239-bp products in two normal female controls. The 239-bp product is normal and the 1364-bp product is aberrant.

that the c.2388+1G>C mutation in *OFD1* is most likely the causal mutation in this family.

X-chromosome inactivation assay

X-chromosome inactivation patterns was random patterns in II-2 available for this study (ratio > 38:62).

Discussion

Exome sequencing detected a single-base substitution (c.2388+1G>C) in *OFD1*, resulting in an error in splicing of intron 17 and a premature stop codon at amino acid position 796, in an affected male (III-5) and a carrier female (II-2) in this family with an 'unclassified' X-linked lethal congenital malformation syndrome. II-4 and III-1, who had strikingly similar clinical manifestations to III-5, are likely to have had the same *OFD1* mutation as III-5, although their DNA was not available. Through reassessment of clinical features of the family, the three affected males shared facial, oral, and digital malformations characteristic of OFD1 (4). Additionally, they exhibited more severe complications in various systems including congenital heart defects, genitourinary malformations, and ophthalmological abnormalities. II-2 was also found to have subtle features of OFD1 (accessory frenulae and irregular teeth). Thus, we have concluded that the 'unclassified' X-linked lethal congenital malformation syndrome in this family was clinically compatible with OFD1.

An *OFD1* mutation (c.2123_2126dupAAGA in exon 16, p.Asn711Lysfs*3) was also detected in a family with an X-linked recessive mental retardation syndrome (10). Nine affected males had macrocephaly and severe mental or developmental retardation, and suffered from recurrent respiratory tract infections leading to early death in eight. Only an 11-year-old boy survived with severe mental retardation (IQ 20), obesity, and brachydactyly. His younger brother had postaxial polydactyly. No cognitive, oral, facial, digital, or renal abnormalities were detected in heterozygous carrier females in that family. The patients were later classified into an infantile lethal variant of Simpson-Golabi-Behmel syndrome (type 2) (SGBS2, OMIM #300209), which had consisted of only one family,

genetically mapped to Xp22, including four maternally related affected males with hydrops at birth, craniofacial anomalies (macrocephaly, low-set posteriorly angulated ears, hypertelorism, short and broad nose with anteverted nares, large mouth with thin upper vermilion border, prominent philtrum, high-arched or cleft palate, and short neck), redundant skin, hypoplastic nails, skeletal defects involving upper and lower limbs, gastrointestinal and genitourinary anomalies, hypotonia and neurological impairment, and early death within the first 8 weeks (11, 12). Other *OFD1* mutations were detected in two families with Joubert syndrome-10 (JBTS10, OMIM #213300) (13). A mutation (c.2844_2850delAGACAAA in exon 21, p.Lys948Asnfs*9) in a family with eight affected males caused severe mental or developmental retardation and recurrent infections in all; postaxial polydactyly in five, retinitis pigmentosa in three, and a molar tooth sign on brain magnetic resonance imaging (MRI) in two. No heterozygous carrier females had any symptoms similar to those in the affected males. Another mutation (c.2767delG in exon 21, p.Glu923Lysfs*4) was found *de novo* in a 12-year-old male patient with severe mental retardation, macrocephaly, obesity, postaxial polydactyly, and a molar tooth sign on brain MRI (13).

To discuss whether these male patients with hemizygous truncating *OFD1* mutations would have different conditions (OFD1, SGBS2, or JBTS10) or belong to the same syndrome spectrum, we have created a comprehensive list of clinical manifestations in all of them (Table 2) (7, 10, 13). Macrocephaly, polydactyly (postaxial), respiratory insufficiency with recurrent respiratory tract infections in survivors, and severe mental or developmental retardation were shared by all the families (7, 10, 13). Nasal bridge features (depressed or broad) and lip abnormalities (cleft lip, pseudocleft lip, full lips, and prominent philtrum) were shared by the families with OFD1 and JBTS10 (7, 13). Brain malformations including hypoplasia or agenesis of corpus callosum, hypoplasia or agenesis cerebellar vermis as well as posterior fossa abnormalities (large, occipital encephalocele) were also shared by the families with OFD1 and JBTS10 (7, 13). III-5 in the present family was described to have Dandy-Walker malformation on brain ultrasonography. Three patients with JBTS10 were described to have a molar tooth sign on brain MRI, which is the characteristic neuroradiological hallmark of Joubert syndrome (13). Dandy-Walker malformation, typically consisting of agenesis or hypoplasia of cerebellar vermis, a cystic dilatation of the fourth ventricle, and an enlarged posterior fossa with a high position of the tentorium, is usually distinguishable from Joubert syndrome, characterized anatomically by agenesis or hypoplasia of cerebellar vermis and enlargement of the superior cerebellar peduncles and deep interpeduncular fossa resulting from a lack of normal decussation of superior cerebellar peduncular fiber tracts, leading to the characteristic 'molar tooth' appearance on transverse computed tomography and MRI of the midbrain (14); and clinically by hypotonia, developmental retardation, abnormal respiratory patterns, and oculomotor apraxia (15). However, Joubert syndrome could be present in association with Dandy-Walker malformation (15); and in such a case, Dandy-Walker malformation was reported to have initially masked the molar tooth sign because of a cystic dilatation of the fourth ventricle (16). Some authors state that the presence of the molar tooth sign does not, in itself, allow a diagnosis, Joubert syndrome, to be made; but that clinical evidence of the syndrome including hypotonia and developmental retardation accompanied by either abnormal breathing or abnormal eye movements should be present (14, 17). Typical respiratory abnormalities in Joubert syndrome, represented by short alternate episodes of apnea and hyperpnea or episodic hyperpnea alone (18), were not described in the patients with JBTS10, with only one presenting with stridor and intermittent cyanosis soon after birth (13). Abnormal eye movements including oculomotor apraxia were not mentioned in those with JBTS10 (13). In view of these evidences, it is reasonable to consider that the male patients with *OFD1* mutations, identified to date, would belong to a clinical continuum with wide intra- and inter-familial phenotypic variations of a single disorder.

A review by Macca and Franco (4) summarized all reported mutations in OFD1 patients. In total, 99 different mutations (7 genomic deletions and 92 point mutations) were identified, including 67 frameshift mutations (58%), 14 missense mutations (12%), 14 splice-site mutations (12%), 13 nonsense mutations (11%), and an in-frame deletion. Point mutations occur only in the first 17 exons (*OFD1* consists of 23 exons). A significant genotype–phenotype correlation between high-arched/cleft palate and missense and splice-site mutations has been identified (19). In addition, cystic kidney is more frequently associated with mutations in exons 9 and 12 (19). Quantitative PCR analysis of *OFD1* mRNA levels in EBV-LCLs from two families with JBTS10 showed that 30% and 58% of *OFD1* expression remained, suggesting that the mutant mRNA would be subject to nonsense-mediated decay and that the phenotypic variability observed for *OFD1* mutations would be caused by changes in activity of remaining truncated OFD1 protein (13). To date, premature stop codons at 713 in exon 16 (19), 796 in exon 17 (this report), 926 in exon 21 (13), and 956 in exon 21 (13) are associated with survival in males with hemizygous truncating *OFD1* mutations and no or subtle clinical manifestations in females with heterozygous *OFD1* mutations. Heterozygous truncating *OFD1* mutations preserving normal exons 1–16 have been reported in only two families with typical female OFD1 patients: a single-base deletion (c.2349delC in exon 17, p.Ileu784Serfs*85) (20) and a deletion of complete exon 17 (21). Mutations producing longer truncated protein (~ exon 17) might cause a milder form of the disorder that could not be detected in typical female OFD1 patients, but could be detected in male patients with multiple congenital anomalies and probable lethality in childhood.

Table 2. Clinical features of male patients with *OFD1* mutations

	Family 1 (present family)			Family 2[b]	Family 3[c]				Family 4[d] (W07-713)			Family 5[d]	Carrier
Patient	II-4	III-1	III-5	1	IV-1	IV-3	IV-11	6 Patients	III-9	IV-10	6 Patients	(UW87)	19 Females
Age	0d/D	14d/D	1d/D		11 y	18 m/D	3 y/D	D	34 y	3.5 y	D (3)		
Birth weight (g) (gestational age)	2056 (33)	3064 (39)	1704 (32)		3850 (40)	4120 (38)	1915 (35)			3050 (Te)		4090 (41)	
Macrocephaly (>1.5 SD)	+		+		+	+	+	Some				+	
Obesity					+				−	−	−	+	
Craniofacial (87.3%[a])									−	−	−		
Facial anomalies (69.1%[a])													
Prominent forehead	+		+										
Redundant neck skin	+											+	
Hypertelorism	+	+	+	+									
Epicanthus		+											
Short palpebral fissures	+	+											
Nasal bridge features	Dep		Dep						Br	Br		Dep	
Low-set ears	+	+			+				+	+			
Lip abnormalities (32.6%[a])	PCL	CL	PCL	PCL					F_L, PP	F_L, PP		PCL	PCL (1)
Oral													
Palatal abnormalities (49.6%[a])	CSP	CP	CSP	CSP	HP								
Accessory frenulae (63.7%[a])													+ (4)
Tongue abnormalities (84.1%[a])	Nar											MG	Lob (3)
Teeth abnormalities (43.3%[a])													Ir (1)
Skeletal													
Short fingers/brachydactyly					+		+			−		+	
Postaxial polydactyly (3.7%[a])	LtH	BiH		BiHRtBLT		RtH			−	BiHF	BiHF (4)	BiHLtF	
Preaxial polydactyly (19.3%[a])	BiBrHx	BiF		BiBHx	BiBrT								
Respiratory													
Laryngeal anomalies	+												
Respiratory insufficiency	+	+				+				+			
Recurrent infections					+	+	+	+	+	+	+ (6)	+	
Cardiovascular													
Congenital heart defects	ASD, PDA	AVSD	HLHS	AVSD						−			
Genitourinary													
Cystic kidney	−		−		−	−			−	−	−	−	
Urinary tract abnormalities	HU	EUO											
Genital abnormalities	MP, C												
Gastrointestinal													
Esophageal abnormalities			+										
Ophthalmological													
Microphthalmia/microcornea	+												
Persistent papillary membrane		+											

Table 2. Continued

Patient	Family 1 (present family)			Family 2[b]	Family 3[c]				Family 4[d] (W07-713)			Family 5[d]	Carrier
	II-4	III-1	III-5	1	IV-1	IV-3	IV-11	6 Patients	III-9	IV-10	6 Patients	(UW87)	19 Females
Optic disc coloboma		+											
Optic nerve atrophy												+	
Retinal detachment	+												
Retinitis pigmentosa									+	+	+ (1)	–	
Central nervous system (48.4%[a])													
Hydrocephalus		+	+	+	–	–	+						
Gyrus abnormalities	Hp			PM	–	–	–						
Corpus callosum abnormalities		Ag		Ag	–	–	–					Hp	
Cerebellar vermis abnormalities		Ag	Ag		–	–	–		Hp	Hp			
Thick superior cerebellar peduncles					–	–	–		+	+			
Molar tooth sign					–	–	–		+	+		+	
Dandy-Walker malformation			+		–	–	–						
Posterior fossa abnormalities				L	–	–	–			L		EC	
Developmental/mental retardation					S	S	+	S	S	S	+ (All)	S	

+, present; –, absent; blank, data not available; Ag, agenesis; ASD, atrial septal defect; AVSD, atrioventricular septal defect; BHx, bifid halluces; Bi, bilateral; BLT, bifid little toe; Br, broad; C, cryptorchidism; CL, cleft lip; CP, cleft palate; CSP, cleft soft palate; d, days; D, death; Dep, depressed; EC, encephalocele; EUO, ectopic urethral opening; F, foot/feet; FL, full lips; H, hand(s); HF, hands and feet; HLHS, hypoplastic left heart; Hp, hypoplasia; HP, high palate; HU, hydroureter; Hx, halluces; Ir, irregular; L, large; Lob, lobulated; Lt, left; m, months; MG, midline groove; MP, micropenis; Nar, narrowing of the tip of the tongue; PCL, pseudocleft of the upper lip; PDA, patent ductus arteriosus; PM, polymicrogyria; PP, prominent philtrum; Rt, right; S, severe; Te, term; T, thumbs; y, years.

[a]From Macca and Franco (4).

[b]From Goodship et al. (7).

[c]From Budny et al. (10).

[d]From Coene et al. (13).

High-throughput, next-generation sequencing (NGS) has had a tremendous impact on human genetic research (22). Moreover, techniques enabling enrichment of selected regions enable us to use NGS efficiently and to identify the causative genes for a reasonable number of genetic disorders as well as susceptibility genes for complex diseases and health-related traits (23). In particular, X-linked disorders are good candidates for exome sequencing. We recently identified a nonsense mutation in *MCT8* causing X-linked leukoencephalopathy in a family from only two affected male samples (24). We have also identified two possible but inconclusive missense variants (*L1CAM* and *TMEM187*) in a family with an atypical X-linked leukodystrophy from only two affected male samples (25). In this study, exome sequencing accompanied by appropriate bioinformatics techniques and a co-segregation evaluation successfully revealed a disease-causing mutation in *OFD1*, which could not have been assumed to be a candidate based on the clinical manifestations of the affected male patients. Unbiased rapid screening through these technologies is a powerful method for the detection of mutations in unexpected causative genes in undiagnosed patients with multiple congenital malformations.

In conclusion, we have identified a causative splicing mutation in *OFD1*, through exome sequencing, in a family with three males having an 'unclassified' X-linked lethal congenital malformation syndrome. The affected males manifested severe multisystem complications in addition to the cardinal features of OFD1 and the carrier female showed only subtle features of OFD1. The present patients, as well as the previously reported male patients from four families (one with clinical OFD1; one with SGBS2 and an *OFD1* mutation; two with JBTS10 and *OFD1* mutations), would belong to a single syndrome spectrum caused by truncating *OFD1* mutations, presenting with craniofacial features (macrocephaly, depressed or broad nasal bridge, and lip abnormalities), postaxial polydactyly, respiratory insufficiency with recurrent respiratory tract infections in survivors, severe mental or developmental retardation, and brain malformations (hypoplasia or agenesis of corpus callosum and/or cerebellar vermis and posterior fossa abnormalities).

Acknowledgements

The authors are grateful to the family for their participation in this study. The authors are also thankful to Prof Germana Meroni (Cluster in Biomedicine, Trieste) for mutation analysis of *MID1*, Dr Takeshi Futatani (Department of Pediatrics, Toyama Prefectural Central Hospital, Toyama, Japan), Dr Masahiko Kawabata (Department of Internal Medicine, Toyama Prefectural Central Hospital, Toyama, Japan), and Dr Akio Uchiyama (Department of Pathology, Toyama Prefectural Central Hospital, Toyama, Japan) for collecting clinical information; Dr Gen Nishimura (Department of Radiology, Tokyo Metropolitan Children's Medical Center) for helping radiological assessment; and Miss Junko Kunimi (Department of Medical Genetics, Shinshu University School of Medicine, Matsumoto, Japan) and Dr Shin-ya Nishio (Department of Otolaryngology, Shinshu University School of Medicine, Matsumoto, Japan) for their technical assistance. This work was supported by research grants from the Ministry of Health, Labour and Welfare (T. K., Y. F., H. S., N. Mi., and N. Ma.), the Japan Science and Technology Agency (N. Ma.), the Strategic Research Program for Brain Sciences (N. Ma.) and a Grant-in-Aid for Scientific Research on Innovative Areas (Foundation of Synapse and Neurocircuit Pathology) from the Ministry of Education, Culture, Sports, Science and Technology of Japan (N. Ma.), a Grant-in-Aid for Scientific Research from Japan Society for the Promotion of Science (N. Ma.), a Grant-in-Aid for Young Scientist from Japan Society for the Promotion of Science (H. S. and N. Mi.) and a grant from the Takeda Science Foundation (N. Mi. and N. Ma.). This work was performed at the Advanced Medical Research Center, Yokohama City University, Japan.

Y. T., H. D., H. S., and N. Mi. performed the genetic analysis; T. K., K. H., Y. N., K. W., and Y. F. evaluated clinical aspects of the family, recruited samples, and prepared them for the analysis. Y. T., T. K. and N. Ma. wrote the manuscript.

Ethics approval

The work was approved by the Yokohama City University (Faculty of Medicine) and the Shinshu University (School of Medicine). Patient consent was obtained.

References

1. Papillon-Leage M, Psaume J. Une malformation hereditaire de la muquese buccale: brides et freins anomaux. Rev Stomatol 1954: 55: 209–227.
2. Gorlin RJ, Psaume J. Orofaciodigital dysostosis: a new syndrome. A study of 22 cases. J Pediatr 1962: 61: 520–530.
3. Ferrante MI, Giorgio G, Feather SA et al. Identification of the gene for oral-facial-digital type I syndrome. Am J Hum Genet 2001: 68: 569–576.
4. Macca M, Franco B. The molecular basis of oral-facial-digital syndrome, type 1. Am J Med Genet C 2009: 151C: 318–325.
5. Toriello HV, Franco B. Oral-facial-digital syndrome type I. In: Pagon RA, Bind TD, Dolan CR, Stephans K, Adam MP, eds. GeneReviews at genetests: Medical Genetics Information Resource (database online). Seattle, WA: Copyright, University of Washington, 1993–2011, from http://www.genetests.org. Accessed on July 23, 2011.
6. Morleo M, Franco B. Dosage compensation of the mammalian X-chromosome influences the phenotypic variability of X-linked dominant male-lethal disorders. J Med Genet 2008: 45: 401–408.
7. Goodship J, Platt J, Smith R, Burn J. A male with type I orofaciodigital syndrome. J Med Genet 1991: 28: 691–694.
8. Fontanella B, Russolillo G, Meroni G. MID1 mutations in patients with X-linked Opitz G/BBB syndrome. Hum Mutat 2008: 29: 584–594.
9. Nishimura-Tadaki A, Wada T, Bano G et al. Breakpoint determination of X;autosome balanced translocations in four patients with premature ovarian failure. J Hum Genet 2011: 56: 156–160.
10. Budny B, Chen W, Omran H et al. A novel X-linked recessive mental retardation syndrome comprising macrocephaly and ciliary dysfunction is allelic to oral-facial-digital type I syndrome. Hum Genet 2006: 120: 171–178.
11. Terespolsky D, Farrrell SA, Siegel-Bartelt J, Weksberg R. Infantile lethal variant of Simpson-Golabi-Behmel syndrome associated with hydrops fetalis. Am J Med Genet 1995: 59: 329–333.
12. Brzustowicz LM, Farrell S, Khan MB, Weksberg R. Mapping of a new SGBS locus to chromosome Xp22 in a family with a severe form of Simpson-Golabi-Behmel syndrome. Am J Hum Genet 1999: 65: 779–783.
13. Coene KL, Roepman R, Doherty D et al. OFD1 is mutated in X-linked Joubert syndrome and interacts with LCA5-encoded lebercilin. Am J Hum Genet 2009: 85: 465–481.
14. McGraw P. The molar tooth sign. Radiology 2002: 229: 671–672.
15. Chance PF, Cavalier L, Satran D, Pellegrino JE, Koenig M, Dobyns WB. Clinical nosologic and genetic aspects of Joubert and related syndromes. J Child Neurol 1999: 14: 660–666.

16. Sartori S, Ludwig K, Fortuna M et al. Dandy-Walker malformation masking the molar tooth sign: an illustrative case with magnetic resonance imaging follow-up. J Child Neurol 2010: 25: 1419–1422.
17. Barkovich AJ. Anomalies with cerebellar dysgenesis: vermian dysgenesis. In: Barkovich AJ, ed. Pediatric neuroimaging, 4th edn. Lippincott Williams & Wilkins, Philadelphia 2005: 391–396.
18. Brancati F, Dallapiccola B, Valente EM. Joubert syndrome and related disorders. Orphanet J Rare Dis 2010: 5: 20.
19. Prattichizzo C, Macca M, Novelli V et al. Mutational spectrum of the oral-facial-digital type I syndrome: a study on a large collection of patients. Hum Mutat 2008: 29: 1237–1246.
20. Thauvin-Robinet C, Cossée M, Cormier-Daire V et al. Clinical, molecular, and genotype-penotype correlation studies from 25 cases of oral-facial-digital syndrome type 1: a French and Belgian collaborative study. J Med Genet 2006: 43: 54–61.
21. Thauvin-Robinet C, Franco B, Saugier-Veber P et al. Genomic deletions of *OFD1* account for 23% of oral-facial-digital type 1 syndrome after negative DNA sequencing. Hum Mutat 2008: 30: E320–E329.
22. Shendure J, Ji H. Next-generation DNA sequencing. Nat Biotechnol 2008: 26: 1135–1145.
23. Bamshad MJ, Ng SB, Bigham AW et al. Exome sequencing as a tool for Mendelian disease gene discovery. Nat Rev Genet 2011: 12: 745–755.
24. Tsurusaki Y, Osaka H, Hamanoue H et al. Rapid detection of a mutation causing X-linked leukodystrophy by exome sequencing. J Med Genet 2011: 48: 606–609.
25. Tsurusaki Y, Okamoto N, Suzuki Y et al. Exome sequencing of two patients in a family with atypical X-linked leukodystrophy. Clin Genet 2011: 80: 161–166.

Gain-of-Function Mutations in *RIT1* Cause Noonan Syndrome, a RAS/MAPK Pathway Syndrome

Yoko Aoki,[1,*] Tetsuya Niihori,[1] Toshihiro Banjo,[2] Nobuhiko Okamoto,[3] Seiji Mizuno,[4] Kenji Kurosawa,[5] Tsutomu Ogata,[6] Fumio Takada,[7] Michihiro Yano,[8] Toru Ando,[9] Tadataka Hoshika,[10] Christopher Barnett,[11,12] Hirofumi Ohashi,[13] Hiroshi Kawame,[14] Tomonobu Hasegawa,[15] Takahiro Okutani,[16] Tatsuo Nagashima,[17] Satoshi Hasegawa,[18] Ryo Funayama,[19] Takeshi Nagashima,[19] Keiko Nakayama,[19] Shin-ichi Inoue,[1] Yusuke Watanabe,[2] Toshihiko Ogura,[2] and Yoichi Matsubara[1,20]

RAS GTPases mediate a wide variety of cellular functions, including cell proliferation, survival, and differentiation. Recent studies have revealed that germline mutations and mosaicism for classical RAS mutations, including those in *HRAS*, *KRAS*, and *NRAS*, cause a wide spectrum of genetic disorders. These include Noonan syndrome and related disorders (RAS/mitogen-activated protein kinase [RAS/MAPK] pathway syndromes, or RASopathies), nevus sebaceous, and Schimmelpenning syndrome. In the present study, we identified a total of nine missense, nonsynonymous mutations in *RIT1*, encoding a member of the RAS subfamily, in 17 of 180 individuals (9%) with Noonan syndrome or a related condition but with no detectable mutations in known Noonan-related genes. Clinical manifestations in the *RIT1*-mutation-positive individuals are consistent with those of Noonan syndrome, which is characterized by distinctive facial features, short stature, and congenital heart defects. Seventy percent of mutation-positive individuals presented with hypertrophic cardiomyopathy; this frequency is high relative to the overall 20% incidence in individuals with Noonan syndrome. Luciferase assays in NIH 3T3 cells showed that five RIT1 alterations identified in children with Noonan syndrome enhanced ELK1 transactivation. The introduction of mRNAs of mutant *RIT1* into 1-cell-stage zebrafish embryos was found to result in a significant increase of embryos with craniofacial abnormalities, incomplete looping, a hypoplastic chamber in the heart, and an elongated yolk sac. These results demonstrate that gain-of-function mutations in *RIT1* cause Noonan syndrome and show a similar biological effect to mutations in other RASopathy-related genes.

RAS GTPases are monomeric G proteins with a molecular mass of 20–40 kDa and cycle between a GTP-bound active and a GDP-bound inactive state. The members of the RAS superfamily are structurally classified into at least five subfamilies: RAS, Rho, Rab, Sar1/Arf, and Ran families.[1,2] The Ras subfamily consists of classical RAS proteins (HRAS, KRAS, and NRAS), RRAS, RRAS2 (TC21), RRAS3 (MRAS), RAPs, RAEB, RALs, RIT1, and RIT2 (RIN). RAS proteins interact with multiple effectors, including RAF kinases, phosphatidylinositol 3-kinase (PI-3 kinase), RalGDS, p120GAP, MEKK1, RIN1, AF-6, phospholipase C epsilon, and the Nore-MST1 complex, and activate multiple downstream signaling cascades.[1,2] Of these signaling pathways, the RAS/mitogen-activated protein kinase (RAS/MAPK) signaling pathway plays a central role in cellular proliferation and differentiation.

Noonan syndrome (MIM 163950) is an autosomal-dominant disorder characterized by short stature, distinctive facial features, and congenital heart defects.[3,4] The distinctive facial features include hypertelorism, downslanting palpebral fissures, ptosis, a webbed or short neck, and low-set, posteriorly rotated ears. Congenital heart defects, including pulmonary valve stenosis and atrial septal defects, occur in 50%–80% of individuals. Hypertrophic cardiomyopathy is observed in 20% of affected individuals. Other clinical manifestations include cryptorchidism, mild intellectual disability, bleeding tendency, and hydrops fetalis. The incidence of this syndrome is estimated to be between 1 in 1,000 to 1 in 2,500 live births. Individuals with Noonan syndrome are at risk of juvenile myelomonocytic leukemia (JMML), a myeloproliferative disorder characterized by excessive production of myelomonocytic cells.[4] Noonan syndrome exhibits phenotypic overlap

[1]Department of Medical Genetics, Tohoku University School of Medicine, Sendai 980-8574, Japan; [2]Department of Developmental Neurobiology, Institute of Development, Aging, and Cancer, Tohoku University, Sendai 980-8575, Japan; [3]Department of Medical Genetics, Osaka Medical Center and Research Institute for Maternal and Child Health, Izumi 594-1101, Japan; [4]Department of Pediatrics, Central Hospital, Aichi Human Service Center, Kasugai 480-0392, Japan; [5]Division of Medical Genetics, Kanagawa Children's Medical Center, Yokohama 232-8555, Japan; [6]Department of Pediatrics, Hamamatsu University School of Medicine, Hamamatsu 431-3192, Japan; [7]Department of Medical Genetics, Kitasato University Graduate School of Medical Sciences, Sagamihara 252-0373, Japan; [8]Department of Pediatrics, Akita University School of Medicine, Akita 010-8543, Japan; [9]Department of Pediatrics, Municipal Tsuruga Hospital, Tsuruga 914-8502, Japan; [10]Department of Pediatrics, Tottori Prefectural Central Hospital, Tottori 680-0901, Japan; [11]South Australian Clinical Genetics Service, SA Pathology, Women's and Children's Hospital, North Adelaide, Adelaide, SA 5006, Australia; [12]School of Paediatrics and Reproductive Health, University of Adelaide, Adelaide, SA 5005, Australia; [13]Division of Medical Genetics, Saitama Children's Medical Center, Saitama 339-8551, Japan; [14]Department of Genetic Counseling, Ochanomizu University, Tokyo 112-8610, Japan; [15]Department of Pediatrics Keio University School of Medicine, Tokyo 160-8582, Japan; [16]Division of Neonatal Intensive Care Unit, General Perinatal Medical Center, Wakayama Medical University, Wakayama 641-8510, Japan; [17]Department of Pediatrics, Jikei University School of Medicine, Tokyo 105-8461, Japan; [18]Department of Pediatrics, Niigata Graduate School of Medical and Dental Sciences, Niigata 951-8510, Japan; [19]Division of Cell Proliferation, United Centers for Advanced Research and Translational Medicine, Tohoku University Graduate School of Medicine, Sendai 980-8575, Japan; [20]National Research Institute for Child Health and Development, Tokyo 157-8535, Japan
*Correspondence: aokiy@med.tohoku.ac.jp
http://dx.doi.org/10.1016/j.ajhg.2013.05.021.

with Costello syndrome (MIM 218040) and cardiofaciocutaneous (CFC) syndrome (MIM 115150).

In 2001, Tartaglia et al. identified missense mutations in protein-tyrosine phosphatase, nonreceptor type 11 (*PTPN11* [MIM 176876]), which encodes the tyrosine phosphatase SHP-2 in 50% of individuals with Noonan syndrome.[5] In contrast, loss-of-function or dominant-negative mutations in *PTPN11* have been reported in individuals with Noonan syndrome with multiple lentigines[6] (formerly referred to as LEOPARD [multiple lentigines, electrocardiographic conduction abnormalities, ocular hypertelorism, pulmonic stenosis, abnormal genitalia, retardation of growth, and sensorineural deafness] syndrome [MIM 151100]). To date, germline mutations in *PTPN11*, *KRAS* (MIM 190070), *SOS1* (MIM 182530), *RAF1* (MIM 164760), and *NRAS* (MIM 164790) have been identified in individuals with Noonan syndrome[7–12] (NS1 [MIM 163950], NS3 [MIM 609942], NS4 [MIM 610733], NS5 [MIM 611553], and NS6 [MIM 613224]), and mutations in *SHOC2* (MIM 602775) and *CBL* (MIM 165360) have been identified in two Noonan-syndrome-like syndromes[13–16] (NSLH [MIM 607721] and NSLL [MIM 613563], respectively) (Figure S1, available online). Moreover, we and another group have identified germline mutations in *HRAS* (MIM 190020) in individuals with Costello syndrome[17] and germline mutations in *KRAS*, *BRAF* (MIM 164757), *MAP2K1* (MIM 176872), and *MAP2K2* (MIM 601263) in individuals with CFC syndrome.[18,19] Mutations in *BRAF* have been also identified in a small percentage of individuals with Noonan syndrome (NS7 [MIM 613706]). A line of studies have shown that a group of the above genetic disorders result from dysregulation of the RAS and downstream signaling cascade (RAS/MAPK pathway syndromes, or RASopathies).[20,21] Recently, mosaicism for *KRAS* and *HRAS* mutations has been reported in nevus sebaceous and Schimmelpenning syndrome,[22] further extending a spectrum of diseases with a dysregulated RAS/MAPK pathway.

To identify genetic causes of Noonan syndrome, we recruited 180 individuals with Noonan syndrome or a related phenotype; they were negative for all coding exons in *PTPN11*, *KRAS*, *HRAS*, and *SOS1*; exons 6 and 11–16 in *BRAF*; exons 7, 14, and 17 in *RAF1*; exons 2 and 3 in *MAP2K1* and *MAP2K2*; and exon 1 in *SHOC2*. Further genetic analysis has been conducted according to their first diagnoses.[17,23–29] This study was approved by the ethics committee of Tohoku University School of Medicine. We obtained informed consent from all subjects involved in the study. We sequenced the exomes of 14 individuals whose clinical manifestations had been confirmed to be consistent with Noonan syndrome by trained dysmorphologists. Targeted enrichment was performed with the Agilent SureSelect Human All Exon v.1 Kit for four individuals and with the SureSelect Human All Exon 50Mb kit for ten individuals. Exon-enriched DNA libraries from these 14 individuals were sequenced on the Illumina Hiseq 2000 for 91 bp (v.1 kit) or 101 bp (50Mb kit). The Burrows-Wheeler Aligner (BWA) was used to align the sequence reads to the human genome (UCSC Genome Browser hg19);[30] all BWA parameters were kept at the default settings. After the removal of duplicates from the alignments, realignment around known indels, recalibration, and SNP and indel calling were performed with the Genome Analysis Toolkit (v.1.5).[31] ANNOVAR was used for annotation against the RefSeq database and dbSNP.[32] We identified approximately 10,000 nonsynonymous, nonsense, and splice-site variations and coding indels per individual (Table S1). Filtering steps using variant databases (dbSNP132 and the 1000 Genome Project database) and in-house exome data were carried out, resulting in the identification of 122–282 variants per individual. By visual inspection of the generated data, four heterozygous *RIT1* (MIM 609591; RefSeq accession number NM_006912.5) variants (c.246T>G [p.Phe82Leu], c.265T>C [p.Tyr89His], c.270G>T [p.Met90Ile], and c.284G>C [p.Gly95Ala]) were found in four individuals. Sanger sequencing validated the heterozygous state of the four variants. We did not find any other strong candidate genes in the results of exome sequencing.

RIT1 shares approximately 50% sequence identity with RAS, has an additional N-terminal extension, and does not possess a C-terminal CAAX motif, a specific motif for post-translational modification.[33,34] *RIT1* is located in chromosomal region 1q22 and consists of six exons. We analyzed an additional 166 individuals diagnosed with Noonan syndrome or a related disorder but without mutations in known genes.[17,23–29] Sanger sequencing of all coding exons in *RIT1* in the 166 individuals showed that 13 in 166 individuals had changes. Combining with the 4 in 14 individuals from exome sequencing, a total of nine missense, nonsynonymous mutations were identified in 17 of 180 (9%) individuals who were suspected to have Noonan syndrome or a related disorder (Table 1 and Figures 1A–1L). The identified germline *RIT1* mutations encode alterations located in the G1 domain (c.104G>C [p.Ser35Thr]); the switch I region, involving the G2 domain (c.170C>G [p.Ala57Gly]); and the switch II region, corresponding to RAS (c.242A>G [p.Glu81Gly], c.244T>G [p.Phe82Val], c.246T>G [p.Phe82Leu], c.247A>C [p.Thr83Pro], c.265T>C [p.Tyr89His], c.270G>T [p.Met90Ile], and c.284G>C [p.Gly95Ala]) (Figure S2). Amino acids where alterations are located are conserved among species (Figure S3). The *RIT1* mutations encode alterations clustered in the switch II region. In contrast, *HRAS* germline mutations identified in Costello syndrome are clustered at codon 12 and 13 in the region encoding the G1 domain[17] (Figure 1M). Mutations in parents were not identified in seven families. These mutations are apparently de novo, but biologic confirmation of parentage was not performed. One mutation, c.104G>C, was inherited from a mother with a Noonan syndrome phenotype (Table 1). None of these mutations were identified in 480 controls.

To assess the functional consequences of *RIT1* mutations identified in affected individuals, we introduced a

Table 1. Mutations in *RIT1*, Family Status, and Heart Defects of Mutation-Positive Individuals

Subject	Exon	Nucleotide Change[a]	Amino Acid Change[b]	Father	Mother	HCM[c]	PS[c]	Other Heart Defects[c]
NS414	2	c.104G>C	p.Ser35Thr	WT	p.Ser35Thr	+	–	MVP, MR
KCC27	2	c.104G>C	p.Ser35Thr	NA	NA	+	+	–
NS43	4	c.170C>G	p.Ala57Gly	NA	NA	+	–	MR, TR
NS185	4	c.170C>G	p.Ala57Gly	NA	NA	+	+	ASD, PDA
NS216	4	c.170C>G	p.Ala57Gly	NA	NA	+	–	–
NS402	4	c.170C>G	p.Ala57Gly	WT	WT	+	+	–
NS168	5	c.242A>G	p.Glu81Gly	NA	NA	–	+	VSD
NS410	5	c.244T>G	p.Phe82Val	WT	WT	+	–	–
NS358	5	c.246T>G	p.Phe82Leu	WT	WT	–	+	ASD
NS465	5	c.246T>G	p.Phe82Leu	NA	NA	–	+	VSD
NS276	5	c.247A>C	p.Thr83Pro	WT	WT	+	+	PVC
KCC8	5	c.265T>C	p.Tyr89His	NA	NA	+	+	–
KCC38	5	c.270G>T	p.Met90Ile	WT	WT	+	+	ASD, VSD, PDA
NS234	5	c.284G>C	p.Gly95Ala	WT	WT	–	–	ASD
NS265	5	c.284G>C	p.Gly95Ala	WT	WT	+	+	–
Og22	5	c.284G>C	p.Gly95Ala	NA	NA	–	–	–
Og45	5	c.284G>C	p.Gly95Ala	NA	NA	+	+	ASD

PCR primers used for sequencing are shown in Table S3. Nucleotide changes are not located in CpG dinucleotides, suggesting that they exhibit baseline mutation rates with a phenotypic filtering effect and that only these mutations lead to this phenotype. Abbreviations are as follows: WT, wild-type; HCM, hypertrophic cardiomyopathy; PS, pulmonic stenosis; MVP, mitral valve prolapse; MR, mitral regurgitation; TR, tricuspid regurgitation; ASD, atrial septal defect; PDA, patent ductus arteriosus; VSD, ventricular septal defect; PVC, premature ventricular contraction; and NA, not available.
[a]RefSeq NM_006912.5.
[b]RefSeq NP_008843.1.
[c]HCM and heart anomalies were diagnosed by echocardiography.

single-base substitution (p.Ser35Thr, p.Ala57Gly, p.Glu81Gly, p.Phe82Leu, or p.Gly95Ala) identified in individuals with Noonan syndrome into a pCAGGS expression vector[36] harboring *RIT1* cDNA. As an experimental control, cDNAs harboring *RIT1* c.89G>T (p.Gly30Val), c.104G>C (p.Ser35Asn), and c.236A>T (p.Gln79Leu) and *Braf* c.1910T>A (p.Val637Glu) (RefSeq NM_139294), which corresponds to oncogenic p.Val600Glu in humans, were also generated. RIT1 p.Gly30Val and p.Gln79Leu correspond to oncogenic RAS alterations p.Gly12Val and p.Gln61Leu, respectively. We introduced pFR-luc, pFA2-Elk1, phRLnull-luc, and wild-type (WT) or mutant expression constructs of *RIT1* into NIH 3T3 cells to examine the transcriptional activation by ELK1,[18,33] a transcription factor that is activated by MAPK. The results revealed that compared with the WT cDNA, all *RIT1* mutations exhibited significant activation. RIT1 p.Gln79Leu, followed by p.Gly95Ala, p.Ala57Gly, p.Phe82Leu, and p.Glu81Gly, showed the highest ELK1 transactivation, as also shown in a past study[37] (Figure 2A). The c.104G>C (p.Ser35Thr) substitution was identified in two affected individuals. RIT1 p.Ser35Asn, which corresponds to dominant-negative alteration p.Ser17Asn in RAS, has been used as a dominant-negative substitution in cell experiments.[38] To examine the functional consequence of p.Ser35Thr, identified in affected individuals, we compared the ELK1 transactivation in cells expressing p.Ser35Thr and those expressing p.Ser35Asn. Enhanced ELK1 transactivation was observed in cells expressing p.Ser35Thr, but not in cells expressing p.Ser35Asn (Figure 2B). These results suggest that *RIT1* mutations identified in affected individuals were gain-of-function mutations.

RIT1 is expressed ubiquitously in embryonic and adult tissues.[33,34] *Rit1*-null mice have been shown to grow to adulthood without any apparent abnormalities;[39] hence, physiological roles of RIT1 in development remain unknown. To examine the developmental effect of identified mutations, we introduced mRNA of the WT and three *RIT1* mutations (c.236A>T [p.Gln79Leu], c.242A>G [p.Glu81Gly], and c.284G>C [p.Gly95Ala]) into 1-cell-stage zebrafish embryos and observed the phenotype at 11 hr postfertilization (hpf). An oval-shaped egg sack, a typical manifestation of the gastrulation defect, was observed in embryos expressing RIT1 alterations (Figure 3A). This characteristic shape change was also observed in zebrafish expressing gain-of-function mutations of human *NRAS*[40]. Next, we observed the phenotype at later stages (48–52 hpf) (Figure 3B and Figure S4). The introduction of the WT mRNA did not interfere with the normal development, resulting in generally normal morphology

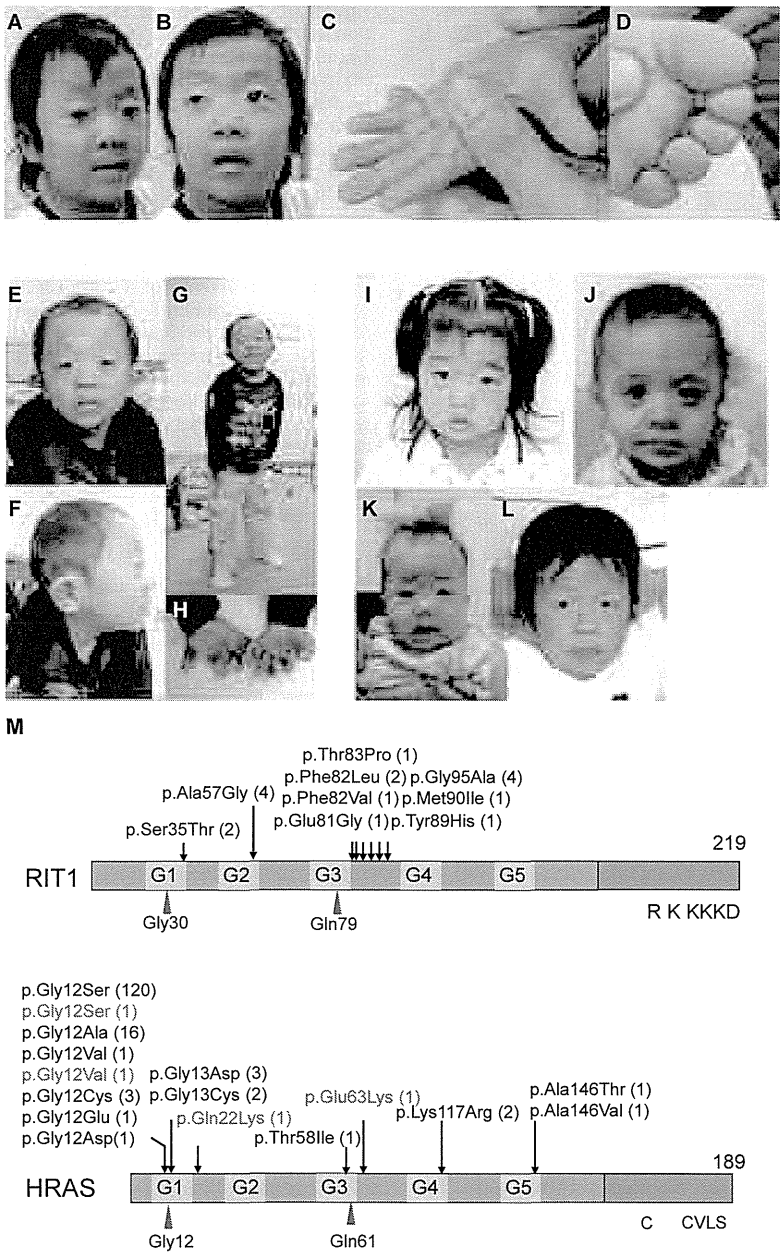

Figure 1. Photographs of Six Individuals in whom *RIT1* Mutations Were Identified
(A–D) KCC38 at 3 years of age. Broad forehead, sparse eyebrows, ptosis, hypertelorism, and hyperpigmentation were observed (A and B). Prominent finger pads were observed (C and D).
(E–H) NS358 at 4 years of age. Hypertelorism, epicanthus, sparse eyebrows, and low-set ears were observed.
(I) NS414 at 3 years of age.
(J) NS465 at 1 year of age.
(K) NS276 at 5 months.
(L) NS265 at 5 years of age.
(M) Structure and identified germline alterations in RIT1 and HRAS. HRAS alterations identified in individuals with Costello syndrome were described before[20] or shown in The RAS/MAPK Syndromes Homepage (see Web Resources). HRAS alterations identified in individuals with congenital myopathy with excess of muscle spindles[35] are indicated in purple.
We obtained specific consent for photographs from six individuals.

in 125/132 (94.7%) embryos; however, 7/132 (5.3%) embryos had limited mild craniofacial and heart abnormalities (Table 2). In contrast, a combined manifestation of craniofacial abnormalities, pericardial edema, and an elongated yolk sac was observed in 66.1%, 52.4%, and 40.5% of embryos expressing p.Gln79Leu, p.Glu81Gly, and p.Gly95Ala, respectively. Development was severely retarded in approximately 7% of embryos expressing RIT1 alterations; these embryos displayed the formation of a disorganized round body shape with a dysmorphic head and body trunk. In the head region, a hypoplastic brain, especially in the telencephalic area, was observed and resulted in misshapen morphology. In the ventral part of the head, the jaw structure was also hypoplastic, and the eyes were translocated medially. These morphological changes gave a cyclopia-like appearance. The ventral sides of the eyes were small, and coloboma along with a loss of pigment was evident (Figure 3B). These phenotypic changes are compatible with the gastrulation defect observed at 11 hpf (Figure 3A). Because the Fgf/Ras/MAPK signaling cascade plays an essential role in the convergent and extension cell movement during gastrulation,[41] perturbation by the RIT1 alterations could cause abnormal cell movement in the axial portions and thus lead to an elongated shape of the egg and the hypoplastic ventral side of the head. Detailed inspection of the morphology in mutant-injected embryos revealed abnormal cardiogenesis, namely, incomplete looping, hypoplastic chambers, and stagnation of blood flow in the yolk sac (Figure 3B). Although the atrium of these hearts beat regularly, the ventricle seemed to twitch passively by the contraction of the atrium (Movies S1, S2, S3, S4, S5, and S6). These results indicate that activating mutations in *RIT1* induce abnormal craniofacial and heart defects in zebrafish.

RIT1-mutation-positive individuals showed a distinct facial appearance, congenital heart defects, and skeletal

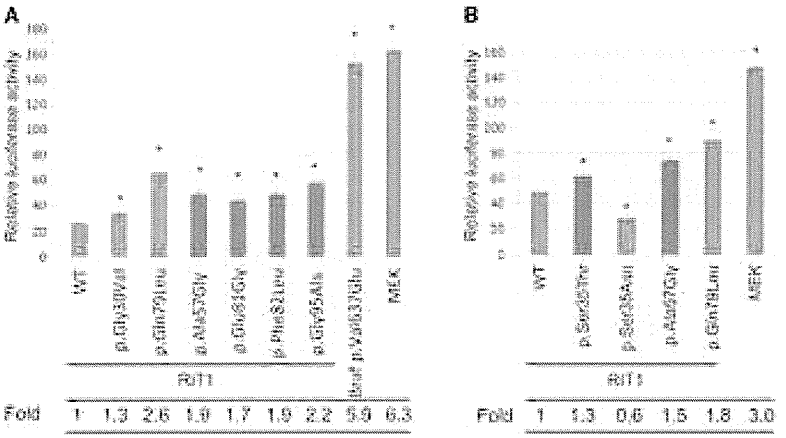

Figure 2. Stimulation of ELK Transcription in NIH 3T3 Cells Expressing *RIT1* Germline Mutations

(A) The ELK1-GAL4 vector and the GAL4 luciferase *trans*-reporter vector were transiently transfected with various *RIT1* germline mutations and activating mutations in *BRAF* and *MAP2K1* in NIH 3T3 cells. c.1910T>A (p.Val637Glu) in mouse *Braf* corresponds to oncogenic c.1799T>A (p.Val600Glu) in human *BRAF*. Relative luciferase activity was calculated by normalization to the activity of a cotransfected control vector, phRLnull-luc, containing distinguishable *R. reniformis* luciferase.

(B) ELK1 transactivation in cells expressing p.Ser35Thr, identified in individuals with Noonan syndrome, and p.Ser35Asn, were examined. p.Ser35Asn corresponds to dominant-negative alteration p.Ser17Asn in RAS.

Results are expressed as the means of quadruplicate (A) and triplicate (B) samples. Error bars represent the SDs of mean values. Red bars indicate germline *RIT1* mutations identified in Noonan syndrome. The following abbreviation is used: WT, wild-type. *$p < 0.01$ by t test.

abnormalities and were diagnosed with Noonan syndrome by diagnostic criteria developed by van der Burgt (Figures 1A–1L and Table 1).[4] Two individuals (NS358 and KCC38) were suspected to have CFC syndrome in the infantile period because of curly, sparse hair, a high cranial vault, and hypoplasia of the supraorbital ridges. Nine individuals showed perinatal abnormality, including polyhydramnios, nuchal translucency, and chylothorax (Table S2). It is of note that one individual (Og45) showing severe pleural effusion, hypertrophic cardiomyopathy, and hepatomegaly that ended in severe body edema and compromised circulation died 53 days after birth. Seven individuals showed high birth weight, probably as a result of subcutaneous edema, which is a typical manifestation observed in individuals with Noonan syndrome.[4] Out of 17 affected individuals, 16 (94%) had heart defects (Table 1): hypertrophic cardiomyopathy (HCM) in 12 (71%) individuals, pulmonary stenosis in 11 (65%) individuals, and atrial septal defects in 5 (29%) individuals. The incidence of pulmonic stenosis and mild cognitive defects is close to the overall incidence of these features in Noonan syndrome cohorts. By contrast, the incidence of HCM is far greater than in individuals with Noonan syndrome overall (25/118 in Noonan syndrome[42] versus 12/17 in individuals with *RIT1* mutations; $p < 0.0001$ by Fisher's exact test). It is of note that a high frequency of HCM (70%) was also reported in individuals with *RAF1* mutations.[10,11,24] It is possible that RIT1 interacts with RAF1 and that gain-of-function mutations in *RIT1* and *RAF1* exert similar effects in heart development.

Somatic alterations in classical RAS have been identified in approximately 30% of tumors.[43] Noonan syndrome and related disorders confer an increased risk of developing malignant tumors.[20,44] In a summary of the literature, it has been reported that 45 of 1,151 (3.9%) individuals with Noonan syndrome (but with an unknown mutation status) developed malignant tumors.[44] Since molecular analysis became available, gene-specific association with malignant tumors has been revealed. The association with JMML, a myeloproliferative disorder characterized by the excessive production of myelomonocytic cells, has been reported in individuals with *PTPN11*, *CBL*, and *KRAS* mutations. Recent reports showed that two individuals with *SOS1* mutations developed embryonal rhabdomyosarcoma.[45,46] A somatic *RIT1* variant, c.270G>A (p.Met90Ile), has been identified in lung cancer (COSMIC database). In the present cohort, 1 (NS168) of 17 individuals with *RIT1* c.242A>G (p.Glu81Gly) developed acute lymphoblastic leukemia at the age of 5 years. The child was treated by a standard protocol and has remained in complete remission. Examining whether gain-of-function mutations in *RIT1* cause tumorigenesis will require further study.

RIT1 has been isolated as a cDNA encoding highly conserved G3 and G4 domains of RAS proteins[33] or identified as a gene encoding a protein related to *Drosophila Ric*, a calmodulin-binding RAS-related GTPase.[34] RIT1 p.Gln79Leu, which corresponds to RAS p.Gln61Leu, is implicated in transforming NIH 3T3 cells, neurite outgrowth in neuronal cells, and the activation of ERK and p38 MAPK in a cell-specific manner.[37,38,47] In this study, enhanced ELK1 transactivation was observed in cells expressing mutant *RIT1* cDNAs. Previous studies showed that enhanced ELK transactivation was observed in NIH 3T3 cells expressing *HRAS*, *KRAS*, *BRAF*, and *RAF1* mutations identified in individuals with Costello, CFC, and Noonan syndromes.[17,18,24] Gastrulation defects observed in zebrafish embryos expressing RIT1 alterations (p.Glu81Gly, p.Gly95Ala, or p.Gln79Leu) were also reported in zebrafish embryos expressing an activating mutation in *NRAS*, *BRAF*, *MAP2K1*, or *MAP2K2*.[40,48] Taken together, these

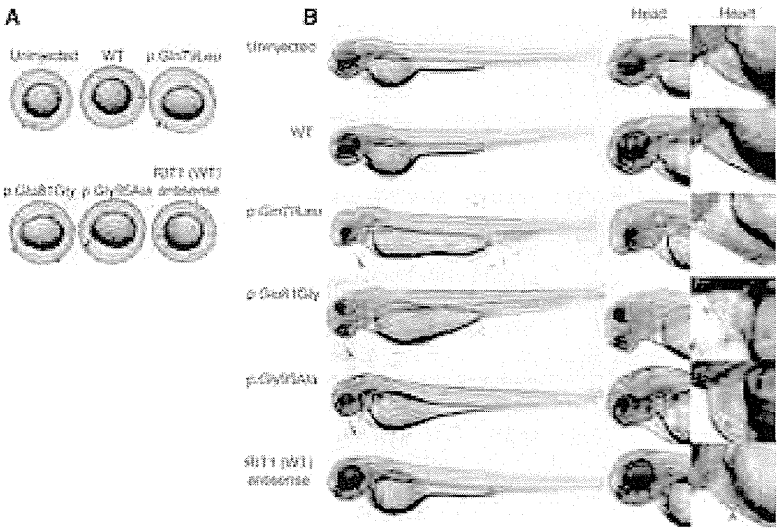

Figure 3. Morphology of Embryos Injected with the WT or Mutant *RIT1* mRNA
In vitro transcription of each mRNA was performed with the mMESSAGE mMACHINE kit (Applied Biosystems) according to the manufacturer's instructions. Synthesized mRNAs were purified with G-50 Micro Columns (GE Healthcare) and subsequently adjusted to a 300 ng/μl concentration for microinjection. Approximately 1 nl (300 pg) of RNA in water with 0.2% phenol red was injected into the cytoplasm of 1-cell-stage zebrafish embryos. Injected embryos were incubated at 28°C until observation.
(A) At 11 hpf, the shapes of the embryos injected with the WT sense or antisense mRNA were round, a normal morphology as observed in the uninjected embryos. In contrast, embryos expressing mutations (c.236A>T [p.Gln79Leu], c.242A>G [p.Glu81Gly], and c.284G>C [p.Gly95Ala]) are oval and compressed along the dorsal-ventral axis, indicative of a gastrulation defect. Note that cells have a hump in the head region at the anterior end of the body axis, the earliest manifestation of a craniofacial defect.
(B) Lateral views at 48 hpf are shown. Embryos expressing mutations (c.236A>T [p.Gln79Leu], c.242A>G [p.Glu81Gly], and c.284G>C [p.Gly95Ala]) formed swollen yolk sacs equally along the anterior posterior axis but did not show narrowing in the caudal half, which was clearly visible in the uninjected embryos and in those injected with the WT sense or antisense mRNA. In the craniofacial area, misshapen head and jaw structures and small eyes with hypoplasia on the ventral side were observed (middle panel); these phenotypes are consistent with the gastrulation defect. Shapes of the hearts (highlighted by red dotted lines) are shown in the right panel at a higher magnification. Normal looping of the heart tube and correct formation of two distinct chambers are observed in embryos injected with the WT sense or antisense mRNA. When mutations (c.236A>T [p.Gln79Leu], c.242A>G [p.Glu81Gly], and c.284G>C [p.Gly95Ala]) were expressed, looping was incomplete, resulting in stretched straight heart tubes. Constrictions at the atrial-ventricular canal are obscure, and the heart chambers are hypoplastic. Abbreviations are as follows: A, atrium; and V, ventricle.

results indicate that gain-of-function mutations in *RIT1* cause Noonan syndrome and show a similar effect to mutations in other RASopathy-related genes in human development.

Herein, we used whole-exome sequencing to identify germline *RIT1* mutations in individuals with Noonan syndrome, a disorder of the RASopathies. Mutations in *PTPN11*, *SOS1*, *RAF1*, *KRAS*, *BRAF*, and *NRAS* have been identified in 41%, 11%, 5%, 1%, 0.8%, and 0.2% of all cases, respectively,[3] and thus the frequency of *RIT1* mutations in Noonan syndrome might be similar to that of *RAF1* mutations. Our findings will improve diagnostic accuracy of Noonan syndrome and provide a clue to understanding the disorder's pathogenesis, including therapeutic approaches.

Supplemental Data

Supplemental Data include four figures, three tables, and six movies and can be found with this article online at http://www.cell.com/AJHG/.

Acknowledgments

The authors thank the families and the doctors who participated in this study. We are grateful to Jun-ichi Miyazaki at Osaka University for supplying the pCAGGS expression vector. We thank Yoko Narumi, Tomoko Kobayashi, Shoko Komatsuzaki, Yu Abe, Yuka Saito, Rumiko Izumi, Mitsuji Moriya, and Masako Yaoita for contributing to routine diagnostic work and Yoko Tateda, Kumi Kato, and Riyo Takahashi for their technical assistance. We are grateful to Eric Haan for sending samples of Noonan syndrome

Table 2. Morphologic Abnormality at 48–52 hpf of Zebrafish Embryos Injected with WT or Mutant RNA at the 1-Cell Stage

	No Abnormalities	Heart and Facial Abnormalities[a]	Severely Disorganized[b]	Total Number of Embryos
WT	125	7 (5.3%)	0 (0%)	132
p.Gln79Leu	31	78 (66.1%)	9 (7.6%)	118
p.Glu81Gly	42	55 (52.4%)	8 (7.6%)	105
p.Gly95Ala	44	34 (40.5%)	6 (7.1%)	84

[a]Craniofacial abnormalities, pericardial heart edema, and an elongated yolk sac were observed.
[b]Disorganized round body shape with a dysmorphic head and body trunk as shown in Figure S4.

and related disorders. We also acknowledge the support of the Biomedical Research Core of Tohoku University Graduate School of Medicine. This work was supported by the Funding Program for the Next Generation of World-Leading Researchers (NEXT Program) from the Ministry of Education, Culture, Sports, Science, and Technology of Japan (MEXT) to Y.A. (LS004), by Grants-in-Aids from MEXT, from the Japan Society for the Promotion of Science, and from the Ministry of Health, Labor, and Welfare to Y.M. and T.N. This work was supported in part by the National Cancer Center Research and Development Fund (23-22-11).

Received: April 23, 2013
Revised: May 19, 2013
Accepted: May 23, 2013
Published: June 20, 2013

Web Resources

The URLs for data presented herein are as follows:

Catalogue of Somatic Mutations in Cancer (COSMIC), http://www.sanger.ac.uk/genetics/CGP/cosmic/
Online Mendelian Inheritance in Man (OMIM), http://www.omim.org
RefSeq, http://www.ncbi.nlm.nih.gov/RefSeq
The RAS/MAPK Syndromes Homepage, http://www.medgen.med.tohoku.ac.jp/RasMapk%20syndromes.html

References

1. Takai, Y., Sasaki, T., and Matozaki, T. (2001). Small GTP-binding proteins. Physiol. Rev. *81*, 153–208.
2. Giehl, K. (2005). Oncogenic Ras in tumour progression and metastasis. Biol. Chem. *386*, 193–205.
3. Romano, A.A., Allanson, J.E., Dahlgren, J., Gelb, B.D., Hall, B., Pierpont, M.E., Roberts, A.E., Robinson, W., Takemoto, C.M., and Noonan, J.A. (2010). Noonan syndrome: clinical features, diagnosis, and management guidelines. Pediatrics *126*, 746–759.
4. van der Burgt, I. (2007). Noonan syndrome. Orphanet J. Rare Dis. *2*, 4.
5. Tartaglia, M., Mehler, E.L., Goldberg, R., Zampino, G., Brunner, H.G., Kremer, H., van der Burgt, I., Crosby, A.H., Ion, A., Jeffery, S., et al. (2001). Mutations in PTPN11, encoding the protein tyrosine phosphatase SHP-2, cause Noonan syndrome. Nat. Genet. *29*, 465–468.
6. Digilio, M.C., Conti, E., Sarkozy, A., Mingarelli, R., Dottorini, T., Marino, B., Pizzuti, A., and Dallapiccola, B. (2002). Grouping of multiple-lentigines/LEOPARD and Noonan syndromes on the PTPN11 gene. Am. J. Hum. Genet. *71*, 389–394.
7. Schubbert, S., Zenker, M., Rowe, S.L., Böll, S., Klein, C., Bollag, G., van der Burgt, I., Musante, L., Kalscheuer, V., Wehner, L.E., et al. (2006). Germline KRAS mutations cause Noonan syndrome. Nat. Genet. *38*, 331–336.
8. Roberts, A.E., Araki, T., Swanson, K.D., Montgomery, K.T., Schiripo, T.A., Joshi, V.A., Li, L., Yassin, Y., Tamburino, A.M., Neel, B.G., and Kucherlapati, R.S. (2007). Germline gain-of-function mutations in SOS1 cause Noonan syndrome. Nat. Genet. *39*, 70–74.
9. Tartaglia, M., Pennacchio, L.A., Zhao, C., Yadav, K.K., Fodale, V., Sarkozy, A., Pandit, B., Oishi, K., Martinelli, S., Schackwitz, W., et al. (2007). Gain-of-function SOS1 mutations cause a distinctive form of Noonan syndrome. Nat. Genet. *39*, 75–79.
10. Pandit, B., Sarkozy, A., Pennacchio, L.A., Carta, C., Oishi, K., Martinelli, S., Pogna, E.A., Schackwitz, W., Ustaszewska, A., Landstrom, A., et al. (2007). Gain-of-function RAF1 mutations cause Noonan and LEOPARD syndromes with hypertrophic cardiomyopathy. Nat. Genet. *39*, 1007–1012.
11. Razzaque, M.A., Nishizawa, T., Komoike, Y., Yagi, H., Furutani, M., Amo, R., Kamisago, M., Momma, K., Katayama, H., Nakagawa, M., et al. (2007). Germline gain-of-function mutations in RAF1 cause Noonan syndrome. Nat. Genet. *39*, 1013–1017.
12. Cirstea, I.C., Kutsche, K., Dvorsky, R., Gremer, L., Carta, C., Horn, D., Roberts, A.E., Lepri, F., Merbitz-Zahradnik, T., König, R., et al. (2010). A restricted spectrum of NRAS mutations causes Noonan syndrome. Nat. Genet. *42*, 27–29.
13. Cordeddu, V., Di Schiavi, E., Pennacchio, L.A., Ma'ayan, A., Sarkozy, A., Fodale, V., Cecchetti, S., Cardinale, A., Martin, J., Schackwitz, W., et al. (2009). Mutation of SHOC2 promotes aberrant protein N-myristoylation and causes Noonan-like syndrome with loose anagen hair. Nat. Genet. *41*, 1022–1026.
14. Loh, M.L., Sakai, D.S., Flotho, C., Kang, M., Fliegauf, M., Archambeault, S., Mullighan, C.G., Chen, L., Bergstraesser, E., Bueso-Ramos, C.E., et al. (2009). Mutations in CBL occur frequently in juvenile myelomonocytic leukemia. Blood *114*, 1859–1863.
15. Niemeyer, C.M., Kang, M.W., Shin, D.H., Furlan, I., Erlacher, M., Bunin, N.J., Bunda, S., Finklestein, J.Z., Sakamoto, K.M., Gorr, T.A., et al. (2010). Germline CBL mutations cause developmental abnormalities and predispose to juvenile myelomonocytic leukemia. Nat. Genet. *42*, 794–800.
16. Pérez, B., Mechinaud, F., Galambrun, C., Ben Romdhane, N., Isidor, B., Philip, N., Derain-Court, J., Cassinat, B., Lachenaud, J., Kaltenbach, S., et al. (2010). Germline mutations of the CBL gene define a new genetic syndrome with predisposition to juvenile myelomonocytic leukaemia. J. Med. Genet. *47*, 686–691.
17. Aoki, Y., Niihori, T., Kawame, H., Kurosawa, K., Ohashi, H., Tanaka, Y., Filocamo, M., Kato, K., Suzuki, Y., Kure, S., and Matsubara, Y. (2005). Germline mutations in HRAS proto-oncogene cause Costello syndrome. Nat. Genet. *37*, 1038–1040.
18. Niihori, T., Aoki, Y., Narumi, Y., Neri, G., Cavé, H., Verloes, A., Okamoto, N., Hennekam, R.C., Gillessen-Kaesbach, G., Wieczorek, D., et al. (2006). Germline KRAS and BRAF mutations in cardio-facio-cutaneous syndrome. Nat. Genet. *38*, 294–296.
19. Rodriguez-Viciana, P., Tetsu, O., Tidyman, W.E., Estep, A.L., Conger, B.A., Cruz, M.S., McCormick, F., and Rauen, K.A. (2006). Germline mutations in genes within the MAPK pathway cause cardio-facio-cutaneous syndrome. Science *311*, 1287–1290.
20. Aoki, Y., Niihori, T., Narumi, Y., Kure, S., and Matsubara, Y. (2008). The RAS/MAPK syndromes: novel roles of the RAS pathway in human genetic disorders. Hum. Mutat. *29*, 992–1006.
21. Tidyman, W.E., and Rauen, K.A. (2009). The RASopathies: developmental syndromes of Ras/MAPK pathway dysregulation. Curr. Opin. Genet. Dev. *19*, 230–236.
22. Groesser, L., Herschberger, E., Ruetten, A., Ruivenkamp, C., Lopriore, E., Zutt, M., Langmann, T., Singer, S., Klingseisen, L., Schneider-Brachert, W., et al. (2012). Postzygotic HRAS and KRAS mutations cause nevus sebaceous and Schimmelpenning syndrome. Nat. Genet. *44*, 783–787.

23. Abe, Y., Aoki, Y., Kuriyama, S., Kawame, H., Okamoto, N., Kurosawa, K., Ohashi, H., Mizuno, S., Ogata, T., Kure, S., et al.; Costello and CFC syndrome study group in Japan. (2012). Prevalence and clinical features of Costello syndrome and cardio-facio-cutaneous syndrome in Japan: findings from a nationwide epidemiological survey. Am. J. Med. Genet. A. *158A*, 1083–1094.
24. Kobayashi, T., Aoki, Y., Niihori, T., Cavé, H., Verloes, A., Okamoto, N., Kawame, H., Fujiwara, I., Takada, F., Ohata, T., et al. (2010). Molecular and clinical analysis of RAF1 in Noonan syndrome and related disorders: dephosphorylation of serine 259 as the essential mechanism for mutant activation. Hum. Mutat. *31*, 284–294.
25. Komatsuzaki, S., Aoki, Y., Niihori, T., Okamoto, N., Hennekam, R.C., Hopman, S., Ohashi, H., Mizuno, S., Watanabe, Y., Kamasaki, H., et al. (2010). Mutation analysis of the SHOC2 gene in Noonan-like syndrome and in hematologic malignancies. J. Hum. Genet. *55*, 801–809.
26. Narumi, Y., Aoki, Y., Niihori, T., Neri, G., Cavé, H., Verloes, A., Nava, C., Kavamura, M.I., Okamoto, N., Kurosawa, K., et al. (2007). Molecular and clinical characterization of cardio-facio-cutaneous (CFC) syndrome: overlapping clinical manifestations with Costello syndrome. Am. J. Med. Genet. A. *143A*, 799–807.
27. Narumi, Y., Aoki, Y., Niihori, T., Sakurai, M., Cavé, H., Verloes, A., Nishio, K., Ohashi, H., Kurosawa, K., Okamoto, N., et al. (2008). Clinical manifestations in patients with SOS1 mutations range from Noonan syndrome to CFC syndrome. J. Hum. Genet. *53*, 834–841.
28. Niihori, T., Aoki, Y., Okamoto, N., Kurosawa, K., Ohashi, H., Mizuno, S., Kawame, H., Inazawa, J., Ohura, T., Arai, H., et al. (2011). HRAS mutants identified in Costello syndrome patients can induce cellular senescence: possible implications for the pathogenesis of Costello syndrome. J. Hum. Genet. *56*, 707–715.
29. Saito, Y., Aoki, Y., Muramatsu, H., Makishima, H., Maciejewski, J.P., Imaizumi, M., Rikiishi, T., Sasahara, Y., Kure, S., Niihori, T., et al. (2012). Casitas B-cell lymphoma mutation in childhood T-cell acute lymphoblastic leukemia. Leuk. Res. *36*, 1009–1015.
30. Li, H., and Durbin, R. (2009). Fast and accurate short read alignment with Burrows-Wheeler transform. Bioinformatics *25*, 1754–1760.
31. McKenna, A., Hanna, M., Banks, E., Sivachenko, A., Cibulskis, K., Kernytsky, A., Garimella, K., Altshuler, D., Gabriel, S., Daly, M., and DePristo, M.A. (2010). The Genome Analysis Toolkit: a MapReduce framework for analyzing next-generation DNA sequencing data. Genome Res. *20*, 1297–1303.
32. Wang, K., Li, M., and Hakonarson, H. (2010). ANNOVAR: functional annotation of genetic variants from high-throughput sequencing data. Nucleic Acids Res. *38*, e164.
33. Lee, C.H., Della, N.G., Chew, C.E., and Zack, D.J. (1996). Rin, a neuron-specific and calmodulin-binding small G-protein, and Rit define a novel subfamily of ras proteins. J. Neurosci. *16*, 6784–6794.
34. Wes, P.D., Yu, M., and Montell, C. (1996). RIC, a calmodulin-binding Ras-like GTPase. EMBO J. *15*, 5839–5848.
35. van der Burgt, I., Kupsky, W., Stassou, S., Nadroo, A., Barroso, C., Diem, A., Kratz, C.P., Dvorsky, R., Ahmadian, M.R., and Zenker, M. (2007). Myopathy caused by HRAS germline mutations: implications for disturbed myogenic differentiation in the presence of constitutive HRas activation. J. Med. Genet. *44*, 459–462.
36. Niwa, H., Yamamura, K., and Miyazaki, J. (1991). Efficient selection for high-expression transfectants with a novel eukaryotic vector. Gene *108*, 193–199.
37. Rusyn, E.V., Reynolds, E.R., Shao, H., Grana, T.M., Chan, T.O., Andres, D.A., and Cox, A.D. (2000). Rit, a non-lipid-modified Ras-related protein, transforms NIH3T3 cells without activating the ERK, JNK, p38 MAPK or PI3K/Akt pathways. Oncogene *19*, 4685–4694.
38. Shi, G.X., and Andres, D.A. (2005). Rit contributes to nerve growth factor-induced neuronal differentiation via activation of B-Raf-extracellular signal-regulated kinase and p38 mitogen-activated protein kinase cascades. Mol. Cell. Biol. *25*, 830–846.
39. Cai, W., Rudolph, J.L., Harrison, S.M., Jin, L., Frantz, A.L., Harrison, D.A., and Andres, D.A. (2011). An evolutionarily conserved Rit GTPase-p38 MAPK signaling pathway mediates oxidative stress resistance. Mol. Biol. Cell *22*, 3231–3241.
40. Runtuwene, V., van Eekelen, M., Overvoorde, J., Rehmann, H., Yntema, H.G., Nillesen, W.M., van Haeringen, A., van der Burgt, I., Burgering, B., and den Hertog, J. (2011). Noonan syndrome gain-of-function mutations in NRAS cause zebrafish gastrulation defects. Dis Model Mech *4*, 393–399.
41. Fürthauer, M., Van Celst, J., Thisse, C., and Thisse, B. (2004). Fgf signalling controls the dorsoventral patterning of the zebrafish embryo. Development *131*, 2853–2864.
42. Burch, M., Sharland, M., Shinebourne, E., Smith, G., Patton, M., and McKenna, W. (1993). Cardiologic abnormalities in Noonan syndrome: phenotypic diagnosis and echocardiographic assessment of 118 patients. J. Am. Coll. Cardiol. *22*, 1189–1192.
43. Schubbert, S., Shannon, K., and Bollag, G. (2007). Hyperactive Ras in developmental disorders and cancer. Nat. Rev. Cancer *7*, 295–308.
44. Kratz, C.P., Rapisuwon, S., Reed, H., Hasle, H., and Rosenberg, P.S. (2011). Cancer in Noonan, Costello, cardiofaciocutaneous and LEOPARD syndromes. Am. J. Med. Genet. C. Semin. Med. Genet. *157*, 83–89.
45. Denayer, E., Devriendt, K., de Ravel, T., Van Buggenhout, G., Smeets, E., Francois, I., Sznajer, Y., Craen, M., Leventopoulos, G., Mutesa, L., et al. (2010). Tumor spectrum in children with Noonan syndrome and SOS1 or RAF1 mutations. Genes Chromosomes Cancer *49*, 242–252.
46. Jongmans, M.C.J., Hoogerbrugge, P.M., Hilkens, L., Flucke, U., van der Burgt, I., Noordam, K., Ruiterkamp-Versteeg, M., Yntema, H.G., Nillesen, W.M., Ligtenberg, M.J.L., et al. (2010). Noonan syndrome, the SOS1 gene and embryonal rhabdomyosarcoma. Genes Chromosomes Cancer *49*, 635–641.
47. Hynds, D.L., Spencer, M.L., Andres, D.A., and Snow, D.M. (2003). Rit promotes MEK-independent neurite branching in human neuroblastoma cells. J. Cell Sci. *116*, 1925–1935.
48. Anastasaki, C., Estep, A.L., Marais, R., Rauen, K.A., and Patton, E.E. (2009). Kinase-activating and kinase-impaired cardio-facio-cutaneous syndrome alleles have activity during zebrafish development and are sensitive to small molecule inhibitors. Hum. Mol. Genet. *18*, 2543–2554.

The European Journal of Orthodontics Advance Access published May 9, 2013

European Journal of Orthodontics
doi:10.1093/ejo/cjt019

Cervical characteristics of Noonan syndrome

Jun J. Miyamoto*, Tomoe Yabunaka* and Keiji Moriyama*,**
*Departments of Maxillofacial Orthognathics, Graduate School and **Global Center of Excellence Program for the International Research Center for Molecular Science in Tooth and Bone Disease, Tokyo Medical and Dental University, Tokyo, Japan

Correspondence to: Keiji Moriyama, Section of Maxillofacial Orthognathics, Graduate School, Tokyo Medical and Dental University, 1-5-45 Yushima, Bunkyo-ku, Tokyo 113-8549, Japan. E-mail: k-moriyama.mort@tmd.ac.jp

SUMMARY

BACKGROUND/OBJECTIVES A short neck and low posterior hairline are characteristics of Noonan syndrome (NS) and are hallmarks of basilar invagination/impression. However, it is seldom that NS has been directly linked with this symptom. Thus, this study aimed to investigate basilar impression in NS subjects compared with control subjects and individuals exhibiting Turner Syndrome (TS).

SUBJECTS/METHODS The degree of basilar impression and vertical positional differences of the third and fourth cervical vertebrae and hyoid bone in NS (n = 9, mean age: 12.1 years), TS (n = 9, mean age: 12.1 years), and control subjects (n = 9, mean age: 12.0 years) were investigated using lateral cephalometric radiographs. Differences between the three groups were compared using the Steel–Dwass test. Vertical positional differences in the anatomical structures within each group were compared using the Wilcoxon signed-rank test accompanied by a Bonferroni–Holm correction.

RESULTS The distance by which the odontoid tip extended past McGregor's line in subjects with NS was significantly greater compared with TS and control subjects. The third and fourth cervical vertebrae were positioned significantly superiorly in subjects with NS compared with TS and control subjects and, in NS, were also significantly superior to the hyoid bone. There was no difference in the position of the hyoid bone itself between the groups.

CONCLUSION/IMPLICATION These results suggest that basilar impression may be a frequently found symptom of NS.

Introduction

Noonan syndrome (NS; OMIM 163950) is an autosomal dominant condition in which approximately 50 per cent of cases are caused by missense mutations in the PTPN11 gene that encodes Shp-2, a regulatory component of the Ras-mitogen-activated protein kinase (Ras-MAPK) signalling network. In contrast, genetic anomalies in other Ras-MAPK pathway genes, such as KRAS, SOS1, and Raf-1, play only a minor role in the molecular pathogenesis of the disease (Ferrero *et al.*, 2008). NS is characterized clinically by a pattern of typical facial dysmorphism, malformations including congenital cardiac defects, short stature, abnormal chest shape, a broad or webbed neck, and a variable learning disability (Turner, 2011; van der Burgt, 2007). Other characteristics are a short neck and low posterior hairline (van der Burgt, 2007). Reduced neck length and low hairline have been recognized as hallmarks of basilar invagination for several decades, and reduced neck length is considered a diagnostic feature of basilar invagination (Goel and Shah, 2009). In a previous study, patients with basilar invagination underwent atlanto-axial joint distraction as a putative treatment modality, with clinical and radiological analysis of the resultant physical and morphological changes in the neck. These experiments suggested that an asymptomatic short neck could be indicative of basilar invagination (Goel and Shah, 2009).

Another reported characteristic feature of NS is malocclusion (Collins and Turner, 1973; Horowitz and Morishima, 1974; Shaw *et al.*, 2007). Thus, patients with NS often have need for orthodontic consultation. Several clinical reports describing such consultations have been published (Asokan *et al.*, 2007; Emral and Akcam, 2009; Ierardo *et al.*, 2010). Other orthodontic studies have reported abnormal radiographic findings in the cervical vertebrae, such as basilar invagination/impression (Vastardis and Evans, 1996; Soni *et al.*, 2008). Such findings during cephalometric analysis were made possible because radiological diagnosis of basilar invagination/impression can be established using constructed lines on the lateral cephalogram (Soni *et al.*, 2008).

It has been previously reported that the Arnold-Chiari malformation is also a characteristic of NS (Peiris and Ball, 1982; Gabrielli *et al.*, 1990; Holder-Espinasse and Winter, 2003; Galarza *et al.*, 2010), but there is only one case study directly linking NS with basilar invagination (Miyoshi *et al.*, 2011). Thus, it is unclear whether basilar invagination/impression is a characteristic of NS.

Turner Syndrome (TS) is a phenotypically similar disorder to NS and shares several NS characteristics, such as short stature, webbed neck, low posterior hairline, and partially similar facial features (Gardner *et al.*, 2007), although the presence of chromosomal defects in the

aetiology of TS distinguish it from NS (van Der Burgt and Brunner, 2000; Delgado-López *et al.*, 2007). Therefore, the aim of this study was to systematically investigate basilar invagination/impression in NS compared with control subjects (lacking any congenital anomalies) and individuals with TS.

Subjects and methods

Subjects

Twenty-seven Japanese subjects participated after giving fully informed consent as required by the protocol, which was approved by the institutional ethics committee (approval #419). Participants were classified into three groups ($n = 9$ in each group): the NS group comprised subjects with NS (five males, four females; mean age: 12.1±2.3 years), the TS group comprised subjects with TS, age-matched to the NS subjects (nine females; mean age: 12.1±2.4 years), and the control group comprised subjects with no congenital anomalies and were age- and gender-matched with subjects in the NS group (five males, four females; mean age: 12.0±2.2 years). Patients with NS and TS were diagnosed at hospitals containing a paediatric department. The karyotypes of TS subjects were unknown. All subjects were devoid of any missing erupted and successional permanent teeth (except for the third molars) and had no cleft lip and/or palate.

Cephalometric analysis

Lateral cephalometric radiographs were taken using a cephalostat (AXIOM Aristos MX/VX; Siemens, Tokyo, Japan). Patients were positioned with teeth in the intercuspal position and with a standing mirror-guided natural head position checked by dental radiologists, such that the degree of basilar impression and any vertical differences in the position of the third and fourth cervical vertebra and the hyoid bone could be simultaneously evaluated. In this study, we measured actual length. The magnification in the lateral cephalometric radiographs is 1.1 times and the results took into account the magnification.

The degree of basilar impression was measured as the distance by which the odontoid tip extended past McGregor's line, drawn from the posterior hard palate to the lowest point on the midline occipital curve (Figure 1). Basilar impression is defined as odontoid tip migration of 4.5 mm or more past McGregor's line (McGregor, 1948).

The vertical positions of the third and fourth cervical vertebra (C3 and C4, respectively) and the hyoid bone (H) were measured by extending a horizontal line from a reference point on each to intersect with a vertical (superior-inferior) line dropped from the sella turcica (S) (Figure 2). These reference points were derived from a previous report describing C3 and C4 references as being the most antero-inferior point of the body of these vertebrae, while the H reference was the most antero-superior point of the body of the hyoid bone (Kollias and Krogstad, 1999; Ricketts, 1989) (Figure 2).

To eliminate experimental errors, the same investigator traced all cephalometric radiographs, and the method error for each parameter was calculated by comparing duplicate tracings at an interval of at least 2 weeks. Errors for a single measurement of linear variables were calculated using the following formula (Dahlberg, 1940):

$$\text{Method error} = \left(\sum \frac{d^2}{2n}\right)^{\frac{1}{2}}$$

where d is the difference between measured pairs and n is the number of pairs.

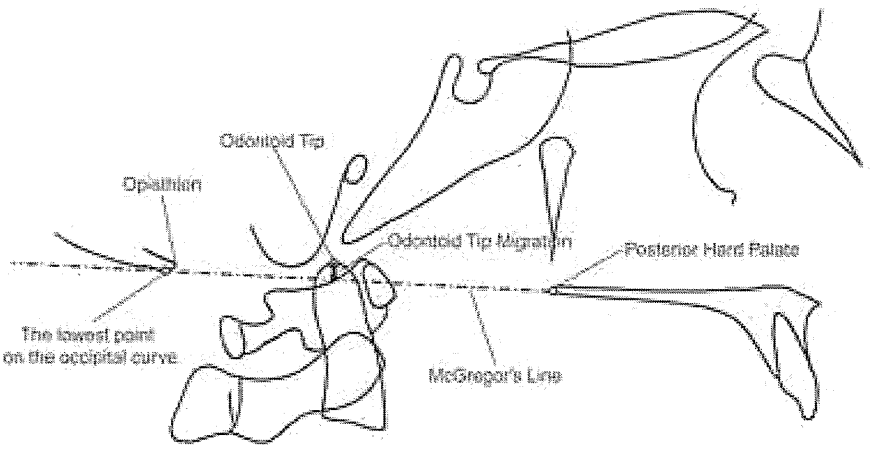

Figure 1 Illustration showing the odontoid tip and McGregor's line, which is used to assess superior odontoid migration. The dashed-dotted lines show McGregor's line, and the distance by which the odontoid tip extends past McGregor's line is indicated by an arrow.

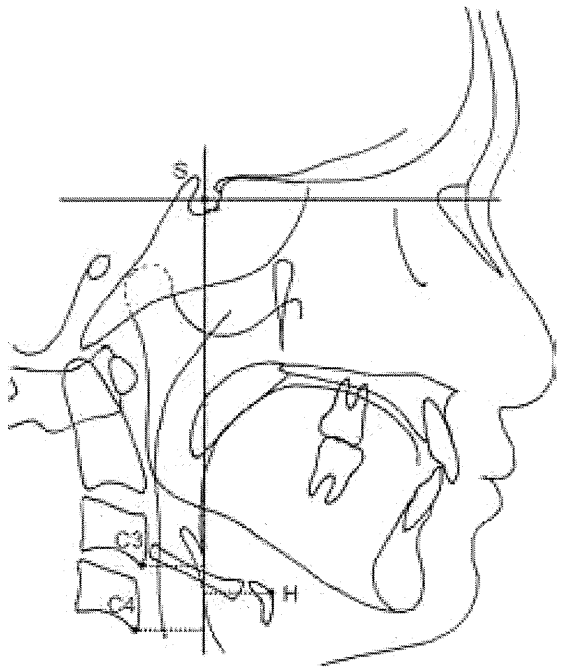

Figure 2 Cervicocraniofacial skeletal reference points used in this study. 'C3', 'C4', and 'H' denote the third cervical vertebra, fourth cervical vertebra, and hyoid bone, respectively. Solid lines show a horizontal line parallel to the floor and a vertical line perpendicular to this horizontal line passing through the sella turcica (S), against which the vertical position of C3, C4, and H can be measured.

Statistical analysis

Differences in linear measurements in the NS, TS, and control groups were examined using a Kruskal–Wallis test with *post hoc* Steel–Dwass analysis, a non-parametric multiple comparison procedure. Differences within each group with regard to the vertical positions of C3, C4, and H were statistically evaluated using the Friedman test and *post hoc* analysis using the Wilcoxon signed-rank test accompanied by a Bonferroni–Holm correction, a non-parametric statistical hypothesis test used when comparing two related or matched samples. A threshold of $P < 0.05$ was considered statistically significant for the Kruskal–Wallis, Steel–Dwass, and Friedman tests, and adjusted P-values were compared with 0.05 using a Wilcoxon signed-rank test with a Bonferroni–Holm correction (Chan *et al.*, 2007).

Results

Representative lateral cephalometric radiographs from the NS, TS, and control groups are shown in Figure 3, with McGregor's line and anatomical structures indicated on each. In the NS group, the odontoid tip, C3, and C4 were all located superiorly to their respective positions in the TS and control groups.

Clinical features of the subjects

Three NS subjects had a short neck and six had a low posterior hairline. In contrast no TS subjects had a short neck, but three TS subjects had a low posterior hairline. Two NS subjects had both symptoms.

Method error

Overall, the mean and standard deviation of the method error was 0.35 ± 0.09 mm for linear measurements. When compared with previous studies (Hiyama *et al.*, 2001), no systematic errors were found.

Degree of basilar impression

Basilar impression is defined as extension of the odontoid tip 4.5 mm or more past McGregor's line (McGregor, 1948). This was the case for seven subjects in the NS group, one subject in the TS group, and no subjects in the control

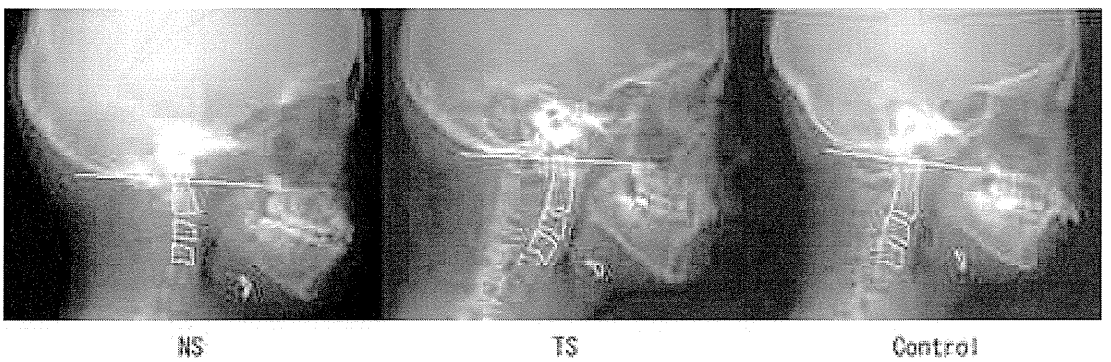

Figure 3 Representative lateral cephalometric radiographs of subjects in the NS, TS, and control groups. White lines denote McGregor's line for each subject. NS, Noonan syndrome; TS, Turner syndrome.

group. The median distance by which the odontoid tip extended past McGregor's line in the NS, TS, and control groups was 7.0, 3.0, and 1.5 mm, respectively (Figure 4A). Statistical analysis using the Kruskal–Wallis test and Steel–Dwass *post hoc* test revealed significant differences between the groups, specifically between the NS and TS or NS and control groups. However, there was no significant difference between the TS and control groups. Between-group comparisons, adjusted for multiple testing by the Steel–Dwass test, are shown in Figure 4B.

Vertical position of the third and fourth cervical vertebrae and the hyoid bone

The Kruskal–Wallis test revealed significant differences between the groups with regard to the vertical position of C3 and C4 but not H. Steel–Dwass comparison showed that the vertical position of C3 was significantly more superior in the NS group compared with the TS and control groups. The same analysis demonstrated no significant difference between the TS and control groups. A similar comparison of the vertical position of C4 revealed it to be significantly more superior in the NS group compared with the TS and control groups. The same analysis demonstrated no significant difference between the TS and control groups. There were no significant differences between the groups with regard to the vertical position of the hyoid bone (H) (Figure 5).

The Freidman test revealed significant differences within each group with regard to the vertical anatomical positions of C3, C4, and the hyoid bone. Comparison of the vertical positions using the Wilcoxon signed-rank test accompanied by a Bonferroni–Holm correction revealed that, in all groups, C3 was located significantly superior to C4. In the NS group, C3 and C4 were located significantly superior to the hyoid bone (Figure 5). In the TS group, C3, but not C4, was located significantly superior to the hyoid bone, whereas in the control group, C3 and C4 were significantly superior and inferior, respectively, in relation to the hyoid bone (Figure 5).

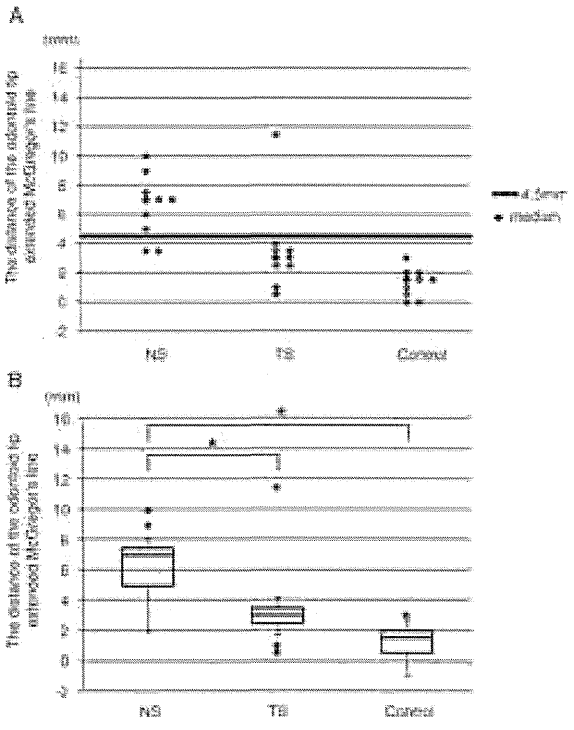

Figure 4 Distance by which the odontoid tip extends past McGregor's line in the NS, TS, and control groups. A, Individual data from all subjects. The horizontal line represents the criterion value of basilar invagination (4.5 mm). B, Data from A are represented as the median value enclosed by the 25th and 75th percentiles (box). Error bars represent 1.5 times the interquartile range of the lower and upper quartile. Data not included between the error bars are plotted as outliers (closed circle). *denotes a significant difference between the groups indicated ($P < 0.05$). NS, Noonan syndrome; TS, Turner syndrome.

Discussion

The present study describes cephalometric analysis aimed at evaluating the position of the cervical vertebrae in NS, TS, and control subjects.

The terms 'basilar impression' and 'basilar invagination' have been used synonymously. Kovero and colleagues defined basilar invagination as a protrusion of the odontoid process into the foramen magnum. This anomaly is apparent from the relation of the dens point to the foramen magnum line (McRae line). The area of the odontoid process that lies above one or several of the reference lines (Chamberlain line, McGregor line, or the baseline for the perpendicular distance from the tip of the odontoid process to a line parallel to the nasion-sella line and drawn through the lowermost point of the posterior cranial base) indicates basilar impression (Kovero *et al.*, 2006). Thus, the term relevant to our results is specified as 'basilar impression', those used in a general sense are specified as 'basilar invagination/impression'.

In the present study, there were three TS subjects with a low posterior hairline, but without basilar impression. Conversely, there were six NS subjects with a low posterior hairline and three with a short neck. Among them, two subjects had both symptoms. One subject with both symptoms and four subjects with a low posterior hairline had basilar impression. In this study, NS subjects with a low posterior hairline were associated with a high probability of basilar impression.

There are currently no reports describing basilar invagination/impression in TS patients. A previous study of basilar invagination/impression in osteogenesis imperfecta (OI) compared 54 OI patients with 108 healthy subjects (Kovero *et al.*, 2006) and found a mean distance of odontoid tip extension past McGregor's line of 2.3 mm in healthy subjects. In the present study, we calculated an equivalent

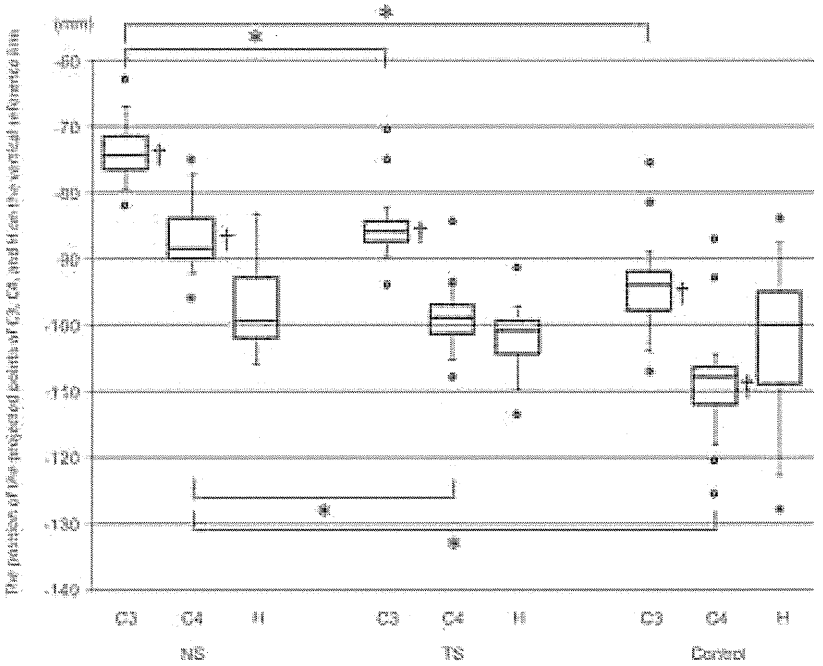

Figure 5 Positions of C3, C4, and H relative to the vertical reference line in the NS, TS, and control groups. The origin of the coordinate axes is the sella turcica and the more inferior the position of the projected point relative to this origin, the smaller the value assigned to it. Data are represented as the median value enclosed by the 25th and 75th percentiles (box). Error bars represent 1.5 times the interquartile range of the lower and upper quartile. Data not included between the error bars are plotted as outliers (closed circle). Asterisk denotes a significant difference between the indicated groups ($P < 0.05$). Dagger symbol denotes a significant difference in the vertical positions between C3 or C4 and the hyoid bone within each group. There were significant differences between C3 and C4 among all groups, but these are omitted from the figure. NS, Noonan syndrome; TS, Turner syndrome; C3, third cervical vertebra; C4, fourth cervical vertebra; H, hyoid bone.

median distance of 1.5 mm in the control group, in reasonable agreement with this previous study, suggesting that our results are comparable to published data.

There is currently only a single report directly linking basilar invagination with NS (Miyoshi *et al.*, 2011). In the present study, the odontoid tip in seven out of nine subjects in the NS group extended 4.5 mm or more past McGregor's line, and the distance by which the odontoid tip extended past McGregor's line in this group was significantly greater compared with the TS and control groups. There are studies that have evaluated basilar invagination/impression using McGregor's line as a reference line. Basilar invagination/impression has been variably defined as the tip of the odontoid process located more than 4.5 (McGregor, 1948), 5 (Soni *et al.*, 2008), and 7 mm (Sillence, 1994) beyond McGregor's line. In the present study, there were seven out of nine subjects (77.8 per cent) with odontoid tip migration of 4.5 mm or more in the NS group, six out of nine subjects (66.7 per cent) with migration more than 5 mm (except one subject with exactly 5 mm), and three out of nine subjects (33.3 per cent) with migration more than 7 mm (except two subjects with exactly 7 mm). In a previous study, it was stated that the odontoid apex should not lie above the criterion distance from McGregor's line in 90 per cent of individuals (Yochum and Lindsay, 2005). In other words, only 10 per cent of subjects would have the odontoid apex below it in the general population. In this study, the percentages of NS subjects with the odontoid apex above it were higher with regard to any of the criteria above.

Basilar invagination/impression is indicative of a cephalad position of the upper cervical vertebra relative to the base of the skull (Guebert *et al.*, 2005). Common signs and symptoms include muscle weakness, neck pain, posterior column dysfunction, bowel and bladder disturbance, and paraesthesia (Goel *et al.*, 1998). However, a large proportion of deformities of the craniovertebral junction, particularly skeletal anomalies, are asymptomatic. Indeed, symptoms were absent in 60 per cent (of 52 cases) of radiologically demonstrable cases of basilar impression (Burrows, 1981), and in 100 per cent of the NS subjects in the present study. The lack of literature reporting coincident NS and basilar invagination/impression may stem from the fact that most NS patients with basilar invagination/impression, being asymptomatic, fail to consult a neurologist.

We found that the positions of C3 and C4, but not the hyoid bone, in the NS group were significantly superior to those in the TS and control groups, suggesting that